Multi-Length Scale Porous Polymers

*Ryu Takekoh and Thomas P. Russell**

Thin films with porosities spanning from the nanoscopic to the macroscopic are obtained by combining breath figures (BFs), micrometer-sized surface cavities arising from the condensation of water on the surface of a film as solvent evaporates rapidly, with the nanoscopic morphology inherent to block copolymers. Using chloroform as a solvent for polystyrene-b-poly methyl methacrylate (PS-b-PMMA) block copolymers (BCPs), micrometer-sized pores arise from the formation of the BFs, while nanoscopic pores are generated by the removal of the PMMA by deep UV-irradiation, which also crosslinks the PS. Solvent retention, though, limits its utility. This is overcome using PS-b-poly(n-butyl methacrylate) dissolved in dichloromethane where, again, multi-length scales of porosity are achieved by a selective removal of one component of BCPs. Arrays of nanopores on the surface of a film can also be obtained by swelling the hydrophilic component block of PS-b-poly(ethyleneoxide) (PEO) with water vapor, under controlled humidity. Simultaneously, large pores can be obtained by macrophase separation between BCPs and water, which leads to multi-length scale porous films.

1. Introduction

Porous polymeric films have uses as membranes,[1] antireflection coatings,[2] as well as in tissue-engineering,[3] and optical devices.[4] To realize these applications, a simple, versatile process to fabricate the porous films is required. Breath figures (BFs) have been studied for the last 20 years to generate porous structures in polymer films from the micrometer to submicrometer size scales,[5–12] Formation of BFs occurs when a polymer solution in a volatile solvent is cast onto a surface. As the solvent evaporates, the surface cools and water on the surface condenses into an ordered array of droplets that do not coalesce. Depending on the contact angle between the water and the solution, and gravitational forces, the water droplets are partially immersed in the solution. In the case of a glassy polymer, as the solvent continues to evaporate, the glass transition temperature increases, exceeds room temperature, and partially encases the droplets. Subsequently, the water evaporates, leaving a hexagonal array of spherically shaped cavities on the surface of the polymer. The size of the pores can be controlled with relative humidity, but the cavities will be sub-micrometer in size when produced by this route.

Block copolymers (BCPs), on the other hand, are ideal templates and scaffolds for the generation of nanoporous materials,[13,14] provided the microdomains can be arranged in a manner to produce continuous pathways through the film. This can be achieved with microdomains oriented normal to the surface, a random orientation of the microdomains where there is a continuous pathway through the film in the minor domains, or by use of gyroid morphology, though this is found only over a narrow range of copolymer compositions. Yet, by combining the self-assembly of BCPs with BF formation, a viable route to multi-length scale structures and morphologies can be realized.

It is, of course, possible to combine the micrometer-sized pores obtained with BFs with the nanoscopic pores from BCPs to generate materials with multi-length scale porous structures. Hayakawa and co-workers fabricated polymer films having micrometer-sized holes and nano-sized phase separated structures by the BFs method using BCPs with a coil-like block and a liquid crystal-containing rod-like block.[15] Rubatat and Billon and co-workers found two levels of organization in polymer films produced by BFs of poly(n-butyl acrylate)-b-polystyrene or poly(tert-butyl acrylate)-b-polystyrene copolymers. These films had a micrometer-sized porous honeycomb structure and the microphase separated morphology characteristics of BCP.[16] Abetz and co-workers produced a film with nano-sized pores on the surface and micrometer-sized pores in thin films by combining classic thin film membrane preparation where a non-solvent-is used to induce a precipitation of the polymer from solution, forming a porous film with a skin on the surface. When the polymer is a BCP, the BCP in the skin will self-assemble into a microphase separated morphology.[17] However, generating a porous polymer film with pores of different size scales that penetrate through the film has yet to be achieved. This would enable control over characteristics, like the refractive index or dielectric constant, throughout the film.

Here, we combined the condensation of water on the surface of a solution as the solvent was evaporating to generate surface topographies. Provided the polymers were hydrophobic, BFs formed on the surface of the solution that were frozen-in

R. Takekoh, Prof. T. P. Russell
IT-related Chemicals Research Laboratory
Sumitomo Chemical Co, Ltd
Ohe-cho, Niihama, Ehime, 792–0015, Japan
E-mail: russell@mail.pse.umass.edu
Prof. T. P. Russell
Department of Polymer Science and Engineering
University of Massachusetts
Amherst, 120 Governors Drive, Amherst, MA 01003, United States
Prof. T. P. Russell
WPI-Advanced Institute for Materials Research (WPI-AIMR)
Tohoku University
2-1-1 Katahira, Aoba, Sendai 980-8577, Japan

DOI: 10.1002/adfm.201301693

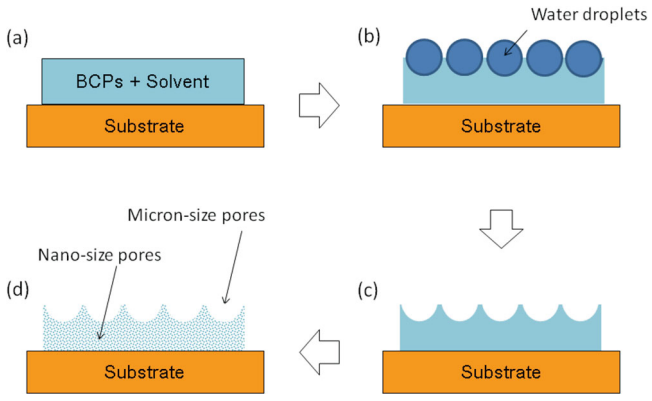

Scheme 1. Schematic representation of the generation of breath figures on the surface of a polymer during solvent evaporation, followed by the removal of the minor component to generate multi-length scale pores in a film.

at the glass transition temperature of the polymer increased about room temperature. By use of BCPs, the removal of the minor component led to multi-length scale porosities in the film (**Scheme 1**).

If one of the blocks was hydrophilic or water soluble, BFs were not formed and the condensed water was solubilized by the minor component block, leading to nanoscopic pores on the surface (**Scheme 2**). Depending on the amount of water absorbed and the evaporation rate of the solvent, fibrillar morphologies formed on the surface, arising from the differences in the solubility of the blocks. These simple processes enable the generation of multiple length scales of porosity in thin polymer films and the fabrication of robust separations media or films with controlled refractive index gradients over a large area.

2. Result and Discussion

Attempts to generate breath figures using PS-b-PMMA have met with limited success. Only over a very limited range of volume fractions of the PS-bock could this be achieved. When the volume fraction of PS was high (>0.7) ordered hexagonal arrays of spherical cavities could be seen in the glassy BCP film. With increasing PMMA content the lateral ordering of the BFs was destroyed and the surface topography became very inhomogeneous. Similar observations were made PMMA and for random copolymers of S and MMA (P(S-r-MMA)) where, for S volume fractions less than 0.82, BFs were not obtained, even at a relative humidity of 85%. Others, however, have reported the formation of BFs using PMMA.[18,19] Park and Kim produced BFs in PMMA by spin coating films from a THF/water solution under a dry environment. However, the surface topographies observed in this study cannot be attributed to BFs but, rather a kinetic trapping of the phase separation of water, THF and PMMA and do not require the condensation of water on the surface during solvent evaporation.[18] Consequently, the hydrophilicity of the polymer and the ability of water to wet the surface upon condensation, such that the droplets are destabilized, appear to be key factors, as reviewed by Stenzel et al.[20] Yet, a detailed explanation of the observation is wanting. While PMMA ($\theta_C = 75°$) is more hydrophilic than PS ($\theta_C = 91°$), water does not wet the PMMA surface. Consequently, the wettability (or lack thereof) of the water on the polymer cannot be the sole origin of the observed BF behavior.

Experiments were performed on PS, poly(n-butylmethacrylate) (PnBMA), PMMA, and poly(2-vinylpyridine) (P2VP) (in increasing order of hydrophilicity). As shown in **Figure 1**, BFs were found in the cases of PS, as also reported by others,[21,22] and PnBMA, but not with PMMA or P2VP (not shown). In addition, the breath figures formed with PnBMA are much smaller. Typically, the sizes of the spherical cavities in the polymer films are 4 µm with PS and 2 µm with PnBMA. In comparison to PS, the BFs formed using PnBMA were not as well-ordered. To understand the relationship between BF formation and the hydrophilicity of the polymer, we investigated the affinity of the polymers for chloroform. If the affinity of the polymer for chloroform is strong, it may affect the rate of solvent evaporation, which causes a cooling of the surface and, consequently, the condensation of water and BF formation. **Figure 2**a shows the absorption rates of thin polymer films for chloroform where the polymer film was placed in the vicinity of a chloroform reservoir in a closed system. The order for the absorption rate and total uptake of chloroform was PS<PnBMA<PMMA<P2VP, indicating that the more hydrophilic polymers have greater affinity for chloroform. The rate

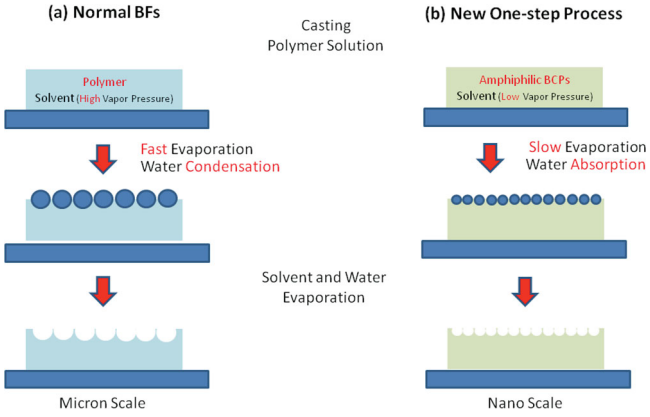

Scheme 2. Schematic representation of process to prepare a nano-honeycomb film in comparison to the traditional method. a) Traditional BFs process. b) One-step process: amphiphilic BCPs and solvent with low vapor pressure are PS-b-PEO and cyclohexanone.

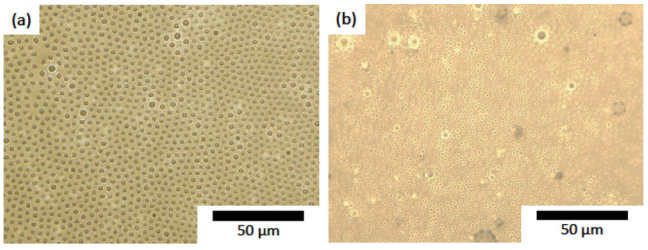

Figure 1. Breath Figures formed on the surface of PS and PnBMA drop cast onto a silicon substrate where the concentration of the solutions were 70 mg mL^{-1} at a relative humidity of 85%.

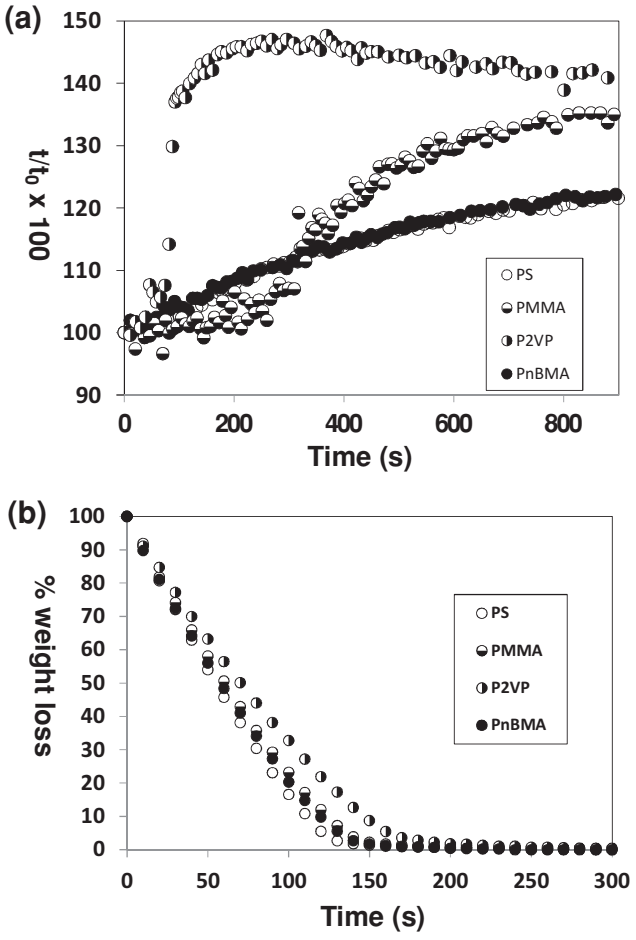

Figure 2. a) Absorption of chloroform, as measured by the change in the film thickness, for PS, PnBMA, P2VP, and PMMA. b) Evaporation of chloroform from swollen films of PS, PnBMA, P2VP, and PMMA.

of chloroform evaporation from a droplet of polymer solution was also examined, as shown in Figure 2b. The order of the evaporation rate of chloroform was PS > PnBMA > PMMA > P2VP which, as would be expected, is exactly in the reverse order of the absorption rate, as a result of the increasing affinity for chloroform. The reduction in the rate of solvent evaporation has two important consequences. First, the lower the evaporation rate, the less cooling of the surface and, therefore, the slower will be the condensation of water. Secondly, the slower the evaporation rate, the lower will be the T_g of the polymer/solvent mixture at the surface, and therefore, the more rapid will be relaxations at the surface. In the absence of a surfactant, the only mechanism for droplet stabilization arises from Marangoni convection during BF formation.[5,23,24] Provided the polymer concentration is low, the choice of polymer does not affect the evaporation rate of the chloroform. With reduced evaporation rate as evidenced by the tailing-off of the evaporation profiles at longer times, thermal gradients will be smaller, and the influence of Marangoni convection is weaker. The residual solvent reduces the viscosity and the glass transition temperature of the solvated polymer film in the late stage of solvent evaporation. This, in turn, leads to either a destabilization of the water droplets on the surface or a behavior where the condensed water droplets evaporate before the effective glass transition temperature of the solvated film increases above the experimental temperature and the surface of the film relaxes. This would be the case for PMMA and P2VP. In case where the BFs are found, the rate of solvent evaporation is more rapid, the surfaces of the films are cooler, and the effective glass transition temperature of the film decreases below the experimental temperature, freezing in the shape of the water droplet before the water evaporates. This would be the case for PS. In the case of PnBMA, it is interesting to note that the size of the BFs for PnBMA are much smaller than those for PS which is consistent with the lower glass transition temperature of PnBMA (T_g = 20 °C), in comparison to that of PS (100 °C). This would result in a lower effective glass transition temperature of the film at the same solvent concentration, allowing more of the condensed water to evaporate before the droplet is frozen-in to the film.

When BCPs have a truly amphiphilic character, they can stabilize water droplets as a surfactant and produce well-ordered BFs.[25] When this is not the case, controlling the affinity of the BCP for the solvent is important for producing BFs. There are at least two ways to change the polymer/solvent affinity. One, of course, is to change the polymer. The second is to change the solvent. It is preferable for solvent to have a weak interaction with both blocks. However, for PS-b-PMMA, a solvent that dissolves both PS and PMMA while also having a weak affinity for these polymers could not be found. Dichloromethane is a good solvent for both blocks and has lower boiling point (41 °C) than chloroform (60 °C), which will reduce the amount of residual solvent at the late stages of BF formation. We also increased the concentration of polymer in the casting solvent. Theoretically, this should not be critical, since, as the solvent is evaporating, the concentration continuously increases. However, the point at which water droplets form on the surface and the viscosity of the polymer film will depend on the initial concentration and could influence the formation of BFs.

With a PS-b-PMMA concentration of 150 mg mL^{-1} at a relative humidity of 85%, BFs with small, densely packed pores were obtained (**Figure 3**a) over small areas (≈2 mm^2). At higher polymer concentrations, the increased viscosity of the polymer solution reduces the tendency for water droplets to aggregate

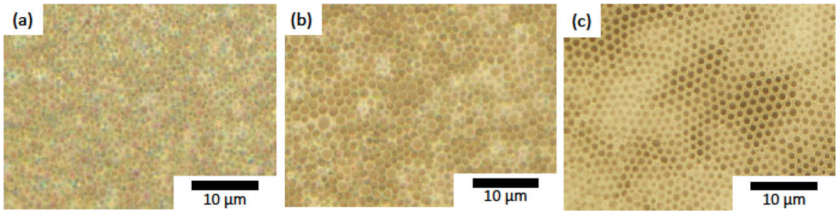

Figure 3. Breath figures formed in PS-b-PMMA (32–30) from a) 150 mg mL^{-1} solution in chloroform at 85% humidity and b) 150 mg mL^{-1} solution in dichloromethane at 55% humidity and in PS-b-PnBMA (43–36) from a 100 mg mL^{-1} solution in dichloromethane at 85% humidity.

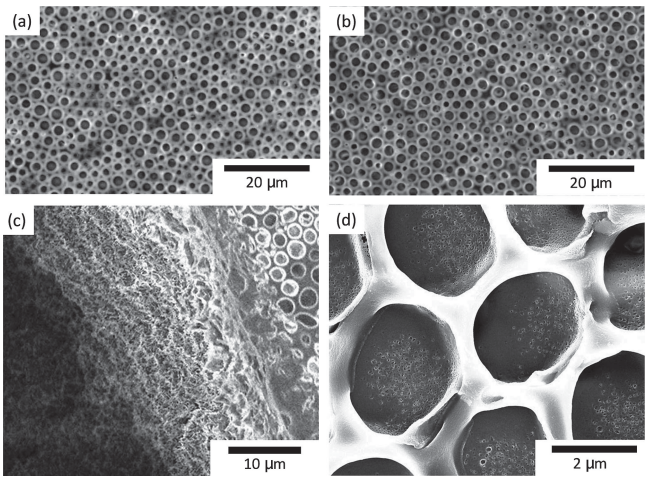

Figure 4. SEM images of BFs of PS-b-PnBMA (43–36) cast from 100 mg mL^{-1} solution of polymer in dichloromethane at 85% humidity a) before and b–d) after exposure to deep UV and rinsing with acetic acid treatment.

or, alternatively, increases the glass transition temperature of the solvated film sufficiently to freeze-in the water droplets before water evaporation. When the solvent was changed from chloroform to dichloromethane, while the quality of the BFs was improved, the overall structure of the BFs was deformed and aggregation of water droplets still occurred. By decreasing the humidity to 55%, the lateral ordering of the BFs was greatly improved, with hexagonally close-packed pores being obtained over larger areas (≈0.2 cm^2), as shown in Figure 3b. To examine the effect of changing the polymer, BFs were produced using PS-b-PnBMA films cast from chloroform. BFs of PS-b-PnBMA from a chloroform solution showed a close-packed structure. By replacing the PMMA with PnBMA, the affinity of the BCP for chloroform decreased and led to a more regularly packed morphology. As with PS-b-PMMA, a higher concentration of PS-b-PnBMA in the casting solution resulted in BFs having a more clearly defined structure over small length scales. In the case where dichloromethane was used, BFs of PS-b-PnBMA with well-ordered structures were obtained over large areas (≈0.5 cm^2) due to the decreased affinity of the BCPs for the solvent and the decrease in the amount of residual solvent in the film at the late stage of BF formation (Figure 3c).

Removal of the PnBMA block from BFs in PS-b-PnBMA deep UV irradiation will degrade the PnBMA and, followed by rinsing with acetic acid, lead to a porous film having two different pore sizes, one on the nanometer (arising from the microphase separation of the PS-b-PnBMA, and the other at the micrometer-scale. There were no substantial differences in BF quality before (**Figure 4**a) and after (Figure 4b) nanopores formation. Nanoscopic pores could be seen in the scanning electron microscopy (SEM) image of a cross-section of the film (Figure 4c) and within the micrometer-sized pores (Figure 4d). While the minimum pore size in the film is dictated by the microphase separated morphology of the BCP, the presence of the large pores arising from the BFs enables a rapid transport of materials through the film.

If the BCP is now made even more amphiphilic, that is, where one block is soluble in water, the opportunity arises to generate nanoscopic BFs where, provided the hydrophilic microdomain is at the surface, water can condense on the hydrophilic microdomain while dewetting the matrix. PS-b-PEO was used to this end, since the morphology of these BCPs has been studied thoroughly in thin films[26,27] and it is known that the morphology of PS-b-PEO is affected by humidity.[28]

With a high vapor pressure solvent, rapid evaporation results in the condensation of water on the surface of polymer solution, resulting in micrometer-sized pores in the film. If, though, a lower vapor pressure solvent is used, the condensation of water droplets can be suppressed and only water absorption by the amphiphilic BCP occurs, leading to nanostructures on the polymer film. Consequently, PS-b-PEO films were cast under high humidity conditions from solvents with low vapor pressure to obtain nanoscopic surface features. Cyclohexanone, a good solvent for both PS and PEO, having a low vapor pressure, was use to cast solutions (70 mg mL^{-1}) of PS-b-PEO (40–35 kg mol^{-1}) at 85% relative humidity. The high humidity serves two purposes. First, since PEO is soluble in water, this high surface energy block is drawn to the surface. The inset in **Figure 5**a shows the concentration of PEO at the surface, as determined by X-ray photoelectron spectroscopy (XPS) on dried films. As can be seen, with increasing humidity, the concentration of PEO at the surface increases. Secondly, water swells the PEO microdomains. At 85% humidity, a nanoscopic honeycomb structure and micrometer-sized domain formed on the surface (Figure 5a). The nanoscopic pores arise from the water, adsorbed in the PEO microdomains, evaporating after the film is dried, and not from the typical BF mechanism. The larger pores are formed from the water droplets that arise due to the high humidity conditions.[25]

The average spacing of the honeycomb structure was 56 nm, which corresponds to that of cylindrical microdomains of PS-b-PEO (51–28), obtained from solvent annealing a thin film of the 51–28 BCP (57 nm) (not shown). This result indicates that the BCP acts as a scaffold for the nanoscopic pores, where

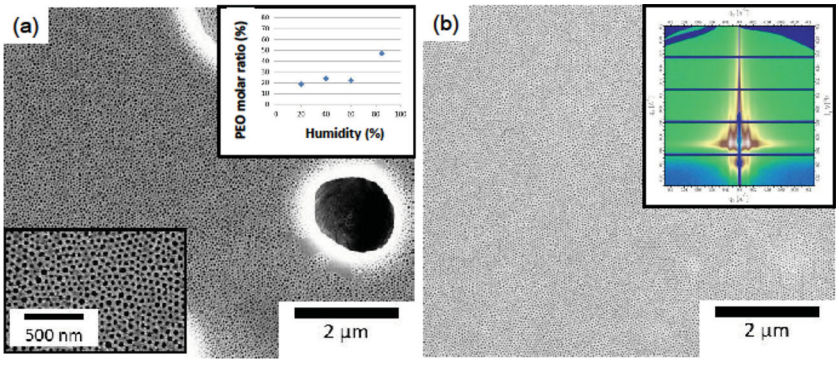

Figure 5. a) Honeycomb pattern formed on the surface of PS-b-PEO (40–35) cast from cylcohexanone. Lower inset is a magnified image. Upper right inset is the mole ratio of PEO on the surface as a function of the relative humidity. b) Blade coated PS-b-PEO (40–35) from cyclohexanone. Inset is the GISAXS pattern from the film.

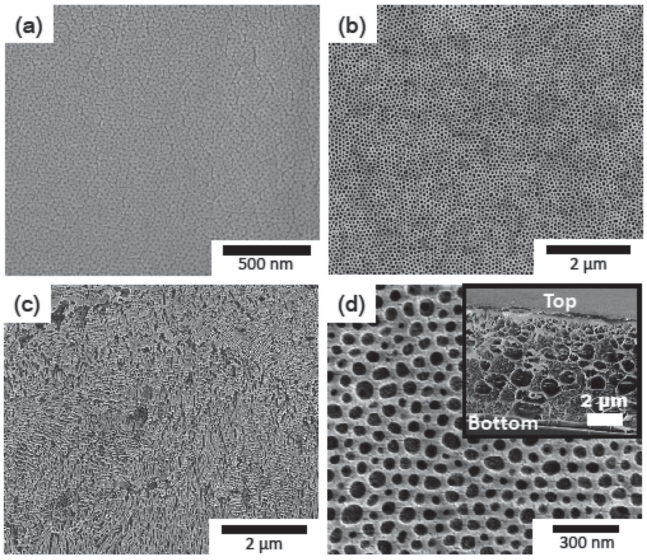

Figure 6. Nanoporous surface on PS-b-PEO cast from cyclohexanone with different molecular weights a) (19–6), b) (59–71), and c) (22–20) cast from 1,-dioxane. d) SEM image PS-b-PEO (40–35) film cast from cyclohexanone/THF/Water (49/49/2 by volume) solution, inset is a cross-section.

the PEO simply absorbs water. If the volume fraction of PEO in the BCP is larger, the film absorbs more water, leading to micrometer-sized pores. Nanoscopic honeycomb structures were obtained over 10 cm^2 area for a 40–35 PS-b-PEO BCP, by blade coating from a solution in cyclohexanone (30 mg mL^{-1}), as shown Figure 5b. Grazing-incidence small-angle X-ray scattering (GISAXS) shows long-range ordering of the honeycomb structure in the polymer film (inset Figure 5b), with a characteristic spacing of 53 nm. This corresponds to measurements obtained from the SEM image (51 nm) and to that from GISAXS (53 nm). The thickness of the film was approximately 200 nm, with the depth of the pores being 30–40 nm. The thickness of the coated solution translates into a longer time for the solvent to evaporate, while the PEO microdomains form on the surface and propagate into the film. The longer evaporation time also provides time for the PEO to absorb water, producing a well-defined surface structure that penetrates into the film.

From these arguments, the molecular weight of the BCP should influence the magnitude of the nanoscopic pores on the surface of the film. **Figure 6**a–c shows SEM images of films obtained from different molecular weights of the PS-b-PEO. When PS-b-PEO (19–6) was cast from cyclohexanone, a film with small honeycomb surface structure with a characteristic distance of 28 nm was obtained (Figure 6a). When PS-b-PEO (59–71) was used, the average separation distance increased to 82 nm (Figure 6b). Consequently, the molecular weight can, in fact, be used to control the size scale of these nanoscopic features, as would be expected. When a symmetric PS-b-PEO (22–20) was cast from 1,4-dioxane, a film with well-defined nanofibers, with an average size of 30 nm, was observed at the surface (Figure 6c). By increasing the molecular weight to PS-b-PEO (59–71), while still maintaining a lamellar microdomain morphology in the bulk, nanofibers with average diameter of 66 nm were obtained (not shown). These results clearly show that the size of nanostructures stem from the molecular weight of the PS-b-PEO BCP template, enabling control of the nanostructures.

Figure 6d shows an SEM image of the hierarchical PS-b-PEO film obtained from 70 mg mL^{-1} cyclohexanone/THF/Water (49/49/2 by volume) solution. A honeycomb structure was present on the surface of the film (Figure 6d), while macroscopic pores were observed within the film (Figure 6d, inset). The morphology on the surface of the film is dictated by the interactions of the blocks with the water and the solvents used, coupled with the evaporation rate of the solvents. THF, miscible with water, evaporates more rapidly than cyclohexanone, and induces a macrophase separation between the BCPs and water, leading to large pores within the film. This is followed by the microphase separation of the BCP throughout the film. Therefore, we can obtain a nano-honeycomb structure on the surface and macropores within the film, in one-step. This, of course, can be converted into fully porous film, with pores ranging from the nanoscopic to macroscopic, by removal of the minor component block. In the case of PEO, for example, a cleavable junction point can be used to this end. This hierarchical film may serve a purpose in the water purification industry,[17,29–31] although further examination would be required to optimize the morphology for this application.

3. Conclusions

We investigated the mechanism of BF formation for PS-b-PMMA and PS-b-PnBMA, from chloroform and dichloromethane solutions. A strong affinity of the polymer for the solvent impedes BF formation with PMMA, P2VP, and PS-b-PMMA, owing to the residual chloroform in the PS-b-PMMA matrix at the late stages of BF formation. This residual solvent depresses the glass transition temperature of the film, allowing the condensed water droplets formed during the evaporation of the solvent to aggregate or fully evaporate while the film is well above its effective glass transition temperature, preventing the formation of BFs. Laterally closely-packed BFs can be formed by manipulating the concentration of the BCP in the initial casting solution or by controlling the BCP/solvent interactions, so that the concentration of the BCP is sufficiently high to freeze-in the droplets before the water droplets evaporate. Removing the minor component of the BCP after the formation of BFs, enables the generation of films, with pores on two different length scales, that have potential applications as separations media, water purification membranes or anti-reflection films. The combination of amphiphilic BCPs and solvent with low vapor pressure allows the film to form a honeycomb structure in a size range too small to be achieved with the standard BFs method. Additionally, polymer films with surface-bound nanofibers were obtained from PS-b-PEO/1,4-dioxane solution. These nanofibers on the surface originated from BCP micelles attributed to the absorption of large amounts of water in 1,4-dioxane during their evaporation. The sizes of these nanostructures were easily controlled by the changing molecular weight of PS-b-PEO, since their

Table 1. Polymers and Block Copolymers.

	M_{Total} [kDa]	$M_{PS(A\text{-}Block)}$ [kDa]	$M_{B\text{-}Block}$ [kDa]	M_w/M_n [kDa]
PS 77K	77	77	0	1.05
PnBMA 77K	77	–	–	1.09
PMMA 60K	60	0	60	1.10
P2VP[a] 71K	71	–	–	1.25
PS-b-PMMA 32–30	62	32	30	1.05
PS-b-PnBMA[b] 43–36	79	43	36	1.08
PS-b-PEO[c] 40–35	75	40	35	1.08
PS-b-PEO 51–28	79	51	28	1.07
PS-b-PEO 19–6	25	19	6	1.05
S-b-PEO 22–20	25	22	20	1.09

[a]P2VP: poly(2-vinylpyridine); [b]PnBMA: poly(n-butylmethacrylate); [c]PEO: poly(ethyleneoxide).

morphologies are determined by the PS-b-PEO template. This novel, one-step method can be extended to other BCPs/solvent systems, and may be amenable to roll-to-roll processing for high volume manufacturing in a variety of industrial fields.

4. Experimental Section

Materials: BCPs, homopolymers, and random copolymers were purchased or synthesized as described in **Table 1**. Chloroform and dichloromethane were purchased from Fisher Scientific Inc. and used as received, without further purification. Cyclohexanone (vapor pressure: 0.5 kPa at 20 °C, boiling point: 155 °C), 1,4-dioxane (vapor pressure: 4.1 kPa at 20 °C, boiling point: 101 °C), and THF (vapor pressure: 19.3 kPa at 20 °C, boiling point: 66 °C) were purchased from Fisher Scientific, Inc.

Film Preparation: The polymers were dissolved in chloroform. 30 µL of the polymer solutions (70 mg mL^{-1}) were placed on a glass slide substrate under high humidity conditions (85% relative humidity) at 20 °C in a humidity-controlled chamber. After complete evaporation of the solvent, the polymer film was removed from the chamber. The PMMA or PnBMA block of the BCP films was removed by irradiation with deep UV light under vacuum, and then rinsed in acetic acid, as necessary.

Characterization: Optical microscopy (OM) measurements were performed in the reflection mode, using an Olympus BX60 microscope to investigate BFs formations. SEM measurements were performed using a FEI Magellan 400 field emission SEM. All samples were coated with 3 nm Au before performing SEM measurements.

To determine the affinity of the homopolymers for chloroform, we performed two different experiments. In the first, the rate of absorption of chloroform was measured in the homopolymer films. Thin films of homopolymers (PS, PMMA, P2VP, and PnBMA), ≈50 nm thick, on a silicon wafer were prepared by spin coating. A 1 cm^2 piece of the thin film was placed in a sealed chamber at 30% relative humidity. After injection of 1 mL chloroform into the chamber through a rubber septum, the variation in the thickness of the polymer film caused by the absorption of chloroform was determined using an optical profilometer (Filmetrix F-20). In a second experiment, the weight loss of polymer film swollen with a solvent was measured as a function of time using an electrobalance at 30% humidity.

X-Ray Photoelectron Spectroscopy: Spectra were obtained with a Physical Electronics Quantum 2000 spectrometer with a 200 µm spot size and monochromatic Al Kα radiation (1486.68 eV). The X-ray source was operated at 50 W and 15 kV with analyzer pass energy of 46.95. eV. Core-level signals were obtained at photoelectron takeoff angles of 45° with respect to the sample surface. Surface compositions were determined by the corresponding core-level spectral area ratios.

Grazing-Incidence Small-Angle X-Ray Scattering: GISAXS measurement was carried out on Beamline 7.3.3 at the Advanced Light Source (ALS) at the Lawrence Berkeley National Laboratory. An X-ray beam impinged onto the sample at a grazing angle of 0.20. The used X-ray wavelength was 1.240 Å, and the scattered intensity was detected by PILATUS 1M detector.

Acknowledgements

This work was supported by the U.S. Department of Energy (DOE), Office of Basic Energy Sciences under contract DEFG02–96ER45612 and by the Sumitomo Chemical Company through a research fellowship for T. Ryu. We thank J.-K. Kim, D. Miranda, K. Bryson, and H.-W. Wang for useful discussions.

Received: May 17, 2013
Published online: October 25, 2013

[1] G. Yang, X. P. Xiong, L. Zhang, *J. Membr. Sci.* **2002**, *201*, 161.
[2] S. Walheim, E. Schaffer, J. Mlynek, U. Steiner, *Science* **1999**, *283*, 520.
[3] T. Nishikawa, J. Nishida, R. Ookura, S. I. Nishimura, S. Wada, T. Karino, M. Shimomura, *Mater. Sci. Eng. C* **1999**, *8*, 495.
[4] J. M. Weissman, H. B. Sunkara, A. S. Tse, S. A. Asher, *Science* **1996**, *274*, 959.
[5] G. Widawski, M. Rawiso, B. Francois, *Nature* **1994**, *369*, 387.
[6] S. A. Jenekhe, X. L. Chen, *Science* **1999**, *283*, 372.
[7] O. Karthaus, N. Maruyama, X. Cieren, M. Shimomura, H. Hasegawa, T. Hashimoto, *Langmuir* **2000**, *16*, 6071.
[8] M. Srinivasarao, D. Collings, A. Philips, S. Patel, *Science* **2001**, *292*, 79.
[9] U. H. F. Bunz, *Adv. Mater.* **2006**, *18*, 973.
[10] P. Escale, L. Rubatat, L. Billon, M. Save, *Eur. Polym. J.* **2012**, *48*, 1001.
[11] M. Hernandez-Guerrero, M. H. Stenzel, *Polym. Chem.* **2012**, *3*, 563.
[12] L. Xue, J. Zhang, Y. Han, *Prog. Polym. Sci.* **2012**, *37*, 564.
[13] M. A. Hillmyer, in *Block Copolymers II*, (Ed:V. Abetz), vol.*190* **2005**, pp 137.
[14] T. Thurn-Albrecht, J. Schotter, C. A. Kastle, N. Emley, T. Shibauchi, L. Krusin-Elbaum, K. Guarini, C. T. Black, M. T. Tuominen, T. P. Russell, *Science* **2000**, *290*, 2126.
[15] T. Hayakawa, S. Horiuchi, *Angew. Chem. Int. Ed.* **2003**, *42*, 2285.
[16] P. Escale, M. Save, A. Lapp, L. Rubatat, L. Billon, *Soft Matter* **2010**, *6*, 3202.
[17] K.-V. Peinemann, V. Abetz, P. F. W. Simon, *Nat. Mater.* **2007**, *6*, 992.
[18] M. S. Park, J. K. Kim, *Langmuir* **2004**, *20*, 5347.
[19] W. Madej, A. Budkowski, J. Raczkowska, J. Rysz, *Langmuir* **2008**, *24*, 3517.
[20] M. H. Stenzel, C. Barner-Kowollik, T. P. Davis, *J. Polym. Sci., Part A* **2006**, *44*, 2363.
[21] A. Boker, Y. Lin, K. Chiapperini, R. Horowitz, M. Thompson, V. Carreon, T. Xu, C. Abetz, H. Skaff, A. D. Dinsmore, T. Emrick, T. P. Russell, *Nat. Mater.* **2004**, *3*, 302.
[22] J. Peng, Y. C. Han, Y. M. Yang, B. Y. Li, *Polymer* **2004**, *45*, 447.

[23] A. V. Limaye, R. D. Narhe, A. M. Dhote, S. B. Ogale, *Phys. Rev. Lett.* **1996**, *76*, 3762.
[24] N. Maruyama, O. Karthaus, K. Ijiro, M. Shimomura, T. Koito, S. Nishimura, T. Sawadaishi, N. Nishi, S. Tokura, *Supramol. Sci.* **1998**, *5*, 331.
[25] K. H. Wong, T. P. Davis, C. Bamer-Kowollik, M. H. Stenzel, *Polymer* **2007**, *48*, 4950.
[26] Z. Q. Lin, D. H. Kim, X. D. Wu, L. Boosahda, D. Stone, L. LaRose, T. P. Russell, *Adv. Mater.* **2002**, *14*, 1373.
[27] S. H. Kim, M. J. Misner, T. Xu, M. Kimura, T. P. Russell, *Adv. Mater.* **2004**, *16*, 226.
[28] J. Bang, B. J. Kim, G. E. Stein, T. P. Russell, X. Li, J. Wang, E. J. Kramer, C. J. Hawker, *Macromolecules* **2007**, *40*, 7019.
[29] F. Schacher, T. Rudolph, F. Wieberger, M. Ulbricht, A. H. E. Mueller, *ACS Appl. Mater. Interfaces* **2009**, *1*, 1492.
[30] E. A. Jackson, M. A. Hillmyer, *ACS Nano* **2010**, *4*, 3548.
[31] A. Jung, S. Rangou, C. Abetz, V. Filiz, V. Abetz, *Macromol. Mater. Eng.* **2012**, *297*, 790.